Volume 16, Issue 1, 162501 (1-12)

International Journal of Nano Dimension (IJND)

https://dx.doi.org/10.57647/j.ijnd.2025.1601.01

First-principles calculations to investigate electronic, optical and thermoelectrical performances of Pb/Te-based nanolayer and bulk chalcogenides

Khadijeh Rajabi[1], Hasan Tashakori [1*], Esmaeil Pakizeh [2*], Fataneh Taghizadeh-Farahmand [1]

[1]*Department of Physics, Faculty of Basic Science, Qom Branch, Islamic Azad University, Qom, Iran.*
[2]*Faculty of Gas and Petroleum, Yasouj University, Gachsaran, Iran.*

[*]**Corresponding authors:** hasan.tashakori@iau.ac.ir, e.pakizeh@yu.ac.ir

Original Research

Received:
24 June 2024
Revised:
29 August 2024
Accepted:
10 September 2024
Published online:
10 January 2025

Abstract:

The electronic,thermoelectric and optical properties of bulk and nanolayers chalcogenides, specifically XTe (X = Si, Ge, Sn, and Pb) and PbY (Y = O, S, Se, and Te), have been investigated using density functional theory (DFT) with the GGA-PBE functional and semiclassical Boltzmann theory via Quantum ESPRESSO and BoltzTraP codes. The results of the electronic band structure analysis indicate that compounds such as PbO, PbS, PbSe, PbTe and GeTe exhibit direct band gaps, making them suitable for semiconductor applications. On the other hand, SiTe and SnTe compounds exhibit metallic behavior. Also, the GeTe bulk was converted from semiconducting to conducting in the nanolayer structure. The thermoelectric properties of these bulk and nanolayerschalcogenides, including electrical conductivity, electronic thermal conductivity, and Seebeck coefficient, have been calculated. It was observed that the Seebeck coefficient decreases with increasing temperature in all semiconductor samples. Moreover, the thermal and electrical conductivity coefficients increase with the increase in chemical potential, transferring it to the electrons in the conduction layer. Based on the findings, it can be concluded that PbTe shows promising potential as a candidate material for thermoelectric devices. Seebeck coefficient in PbO, PbS, and PbSe nanolayers increased compared to the bulk structure. The optical properties, including the real and imaginary parts of the dielectric function, absorption, and reflectivity as a function of energy, have also been calculated. The absorption edges of the bulk chalcogenides extend into the visible spectrum due to their suitable bandgap values. Additionally, these materials exhibit non-transparency in certain regions of the electromagnetic spectrum, making them suitable for use as absorbent materials. Among the chalcogenides studied, PbS shows promising potential for optoelectric industries due to its low refractive index and high optical gap. Also, the decrease in the refractive index of the nanolayers compared to the bulk shows more optical absorption in them. Additionally, among bulks compounds, PbTe shows promising potential for thermoelectric applications, while among nanolayers, PbO is the most suitable material.

Keywords: DFT; Nanolayers; Optical properties; Pb-based chalcogenides; Te-based chalcogenides; Thermoelectric properties

1. Introduction

Today with the progress in nanotechnology, in the context of increasing energy demand, exhaustion of fossil fuels, and global warming, renewable energy sources are becoming increasingly important; these energy sources are clean, sustainable, and can be exploited for thousands of years [1–4]. Among the various types of renewable energy options, such as wind, solar, hydro, and geothermal energy, thermoelectricity is the most environmentally friendly [5]. Thermoelectricity is the field of science that encompasses energy conversion; it converts heat into electrical energy (Seebeck effect) or vice versa, electrical energy into heating or cooling (Peltier effect) [6–8]. Among these two effects, the conversion of heat into electrical energy offers a way to store wasted thermal energy, which has the advantage of being stored in a smaller space for longer periods of time. Given these benefits, researchers are working to develop materials and nanomaterials that exploit the Seebeck and

Peltier effects to extract free, wasted, and renewable energy. This article discusses the extraction of electrical power from waste heat using thermoelectric materials. The fundamentals of the Seebeck effect are also described, along with recent developments in thermoelectric energy conversion with an emphasis on the Peltier effect [6–8]. Additionally, recent research on new materials with various structures (bulk, nanolayer, nanoparticle, nanotube and thin film) for thermoelectric (TE) energy conversion is discussed. The need for high TE efficiency with low engineering costs poses the major challenge in this area. Until now, TE energy extraction was hampered by several factors such as toxicity, low efficiency, and limited availability of certain chemical elements. TE materials should be able to generate the appropriate voltage with arbitrary temperature differences in order to convert heat into electricity. For this purpose, the electrical conductivity (σ) and Seebeck coefficient (S) should be high so that the thermal noise is extremely low. Moreover, the electronic (κ_e) and lattice thermal conductivity (κ_l) should be kept as low as possible to ensure minimal loss of thermal energy. In this article, these properties are examined with the help of the figure of merit, ZT [9–11].

$$ZT = \frac{\sigma S^2 T}{\kappa_e + \kappa_l} \tag{1}$$

At present, almost all of the TE materials have a low ZT value, which is less than 1. This has led to the development of new semiconductors with higher ZT values as the main direction of TE materials research [12–20].

This is because TE materials with a ZT value greater than 1 open up new development directions for the application of TE materials in various industries. The most promising thermoelectric materials are mainly two types: semiconductor alloys and chalcogenides. These materials can be selected according to the temperature range required for applications at any temperature, and finally, a comprehensive decision is made base on the performance [21–25]. For applications at ambient temperatures above 150 ^{O}C, a variety of TE devices based on bismuth telluride (BiTe) materials have been produced [21–25]. For applications in the medium temperature range of 150-500 ^{O}C, a variety of TE devices based on lead telluride (PbTe) materials were produced [26–30]. For medium temperatures above 500 ^{O}C, a variety of TE devices based on silicon germanium (SiGe) materials were produced [30–34]. In recent years, a large number of minerals, organic and phase hybrid TE materials have been reported in the literature to prepare TE devices [35–43]. Among inorganic TE materials, minerals such as Bi_2Te_3, SiGe, PbTe and their alloys exhibit the highest ZT coefficient [44]. For example, the resulting compound Bi_2Te_3 has a ZT value of 0.8 to 1.0 and room temperature (T=300 K) [45]. Early on, research was conducted on how to improve the Seebeck coefficient (S) and electrical conductivity (σ) of tellurium-based chalcogenide TE materials in order to achieve the target ZT [46]. For example, researchers found that PbTe achieves ZT values of 1.4, 1.5 and 1.8 at temperatures of 750, 773 and 850 K, respectively [47–49].

Mishra et al. [50] consider the electronic and TE properties of boron chalcogenide materials BX (X = S, Se, Te) and found that these materials have a good value of ZT close to unity for the temperature range of 200-450 K. The highest value of ZT is about 1.022 in the case of BSe. Also, Gupta et al. [51] investigate the TE properties of the chalcogenide material SnSeS and its defect using the first principle approach in medium temperature range (300-800 K). In this range, they found that $SnSe_{0.7}S_{0.3}$ has the highest ZT [51]. Chalcogenide semiconductors have a significant optical response and are also quite useful for solar cell and infrared detector applications. However, the optical behavior of the solids is related to all the electrons in the materials and not only the free electrons. The dielectric function is an experimental function that is very sensitive to the crystal band structure and hence can be utilized to find out the overall crystal band structure. Several studies are available in the literature, and in the last few years, many articles have been reported on the optical behavior of chalcogenide compounds in different structures [52]. These studies contribute a lot in understanding the optical behavior, future and potential applications for these applications. Azam et al. [53] calculated the optical properties of ternary chalcogenides AlX_2Te_4 (X = Zn, In) using Density Functional Theory (DFT) in the energy range of 0 to 14 eV. Their results indicated that these materials could be a suitable choice for optoelectronic devices. Mathew et al. [54] investigated the optical properties of $BaTiX_3$ (X = S, Se) using DFT+U. Their findings revealed that both materials exhibit significant optical anisotropy for various values of U. Goumri-Said et al. [55] studied the optical properties of ternary selenide chalcogenide Tl_3AsSe_3 using the Modified Becke Johnson (mBJ) approximation. The results of their research demonstrated that this material maintains a positive refractive index, indicating a non-negative refractive index value. Challenging semiconductors have attracted the attention of researchers mainly because of their unique thermoelectric and optical properties. Pb/Te-based chalcogenides have long been known as diverse functional materials and are of interest in nano chemistry today. New and innovative synthesis methods of these compounds in the form of nanowires, nanolayers and nanocrystal networks turn them into materials with interesting and unpredictable properties [56–63].

In this paper, the authors conducted a comprehensive study on the structural, electrical, thermoelectric and optical properties of three-dimensional (bulk) and nanolayers chalcogenides XTe (X=Si, Ge, Sn and Pb) and PbY (Y=O, S, Se, and Te) materials. The nanolayers studied in this article are all monolayers.

The investigation was carried out using DFT with the GGA-PBE functional, as well as semiclassical Boltzmann theory through the utilization of Quantum ESPRESSO and BoltzTraP codes. This study represents the first exploration of these properties for the mentioned materials. These nanolayers have many applications in infrared sensors, military industries, optical filters and ultraviolet absorbers.

2. Computational details

In this article, the properties of XTe and PbY materials were calculated using the DFT method and the Quantum Espresso (QE) simulation code [64]. The self-consistent calculations

Table 1. Calculated equilibrium lattice constant a ^{O}A and coherence energy (eV).

chalcogenides	a (*Å*)	coherence energy(eV)	a (*Å*) others
SiTe	5.843	13.43	-
GeTe	6.024	13.75	5.95 [65]
SnTe	6.389	12.95	6.31 [66]
PbTe	6.574	13.06	6.46 [67]
PbSe	6.229	5.61	6.124 [68]
PbS	6.009	6.65	5.923 [69]
PbO	5.265	8.47	5.51 [70]

Table 2. Structural parameter of bulk Pb/Te-based chalcogenides.

Primitive cell		Conventional cell	
△1-2-3=60 ^{O}C	1-2=4.26 *Å*	△7-8-10=90 ^{O}C	9-11=3.012 *Å*
△1-2-6=90 ^{O}C	1-3=4.26 *Å*	△8-7-9=90 ^{O}C	10-11=3.012 *Å*
△2-6-3=90 ^{O}C	2-6=3.012 *Å*	△7-8=3.012 ^{O}C	7-10=5.2174 *Å*
△3-4-5=120 ^{O}C	1-6=5.217 *Å*	△7-11=4.26 ^{O}C	9-10=4.26 *Å*
△3-6-4=90 ^{O}C	6-4=3.012 *Å*		

(SCF) were performed using the pw.x code from the QE code packages. The parameters used for the SCF calculations included a K-point grid of 12×12×12, an energy convergence limit of 10^{-8} Ry, and a convergence threshold on forces of 10^{-5} Ry/a_0. The kinetic energy cutoff for wave functions and charge density was set to approximately 30 and 300 Ry, respectively. The projected augmented-wave (PAW) pseudopotentials were utilized for the exchange-correlation term in the PBE method [71]. Ultrasoft (USPP) pseudopotentials were employed in all calculations. For the calculations of the electronic band structure, density of states (DOS) and projected density of states (PDOS), the band.x, dos.x and projwfc.x codes were used, respectively. Optical calculations were performed using a larger mesh of 20×20×20 k-points and the epsilon.x code. The thermoelectric properties of the compounds were obtained using the BoltzTrap computational code, which utilizes the semi-classical Boltzmann method. For this purpose, a bulk network with a specified number of wave vector points (20×20×20) was employed.

3. Results and discussion

3.1 Structural and stability properties

The bulk chalcogenides, XTe (X = Si, Ge, Sn, and Pb) and PbY (Y = O, S, Se, and Te), have a cubic (FCC) structure with a primitive unit cell. For all the bulk chalcogenides, the primitive cell contains one Pb/Te atom and one other (X/Y) atom, see figure 1 for the optimized structures of the bulk chalcogenide materials in both the primitive (a) and the conventional (b) unit cells. To determine the equilibrium lattice constant and the coherence energy, the structures were optimized; see Table 1. In the cubic structure, the Pb and Te atoms are positioned at the center of the cube, while one of the X/Y atoms is placed on each face of the cube. The bond length and the atom angles for the materials in both the primitive and the conventional unit cells are given in Table 2. The formation energy of materials indicates their stability. The higher it is, the higher the stability of the materials. The amount of this energy for SiTe, GeTe, SnTe, PbTe, PbSe, PbS, and PbO in nanolayer mode is 14.6426, 14.4522, 14.1343, 14.1974, 7.2355, 7.7503 and 9.7485 eV respectively. The formation energy of SiTe, GeTe, SnTe,

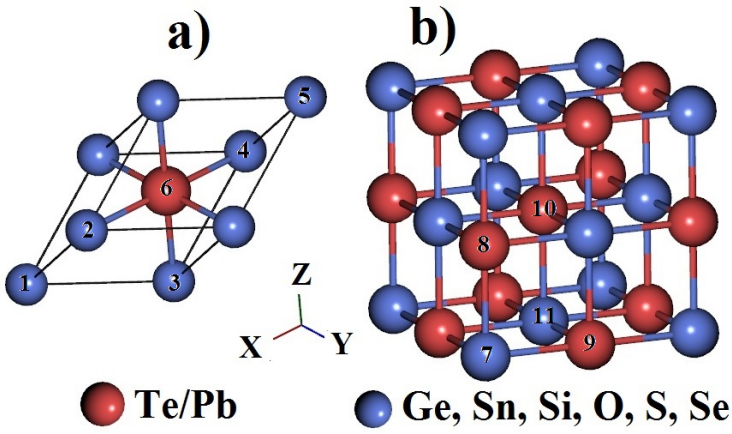

Figure 1. Pb/Te-based chalcogenides structure. a) primitive unit cell, b) conventional unit cell.

PbTe, PbSe, PbS, and PbO in bulk mode is 13.43, 13.75, 12.95, 13.06, 5.61, 6.65, and 8.47 eV, respectively.

3.2 Electronic properties

The band structure was calculated along the symmetric (Γ-W-L-Γ-X-W-K) path of the first Brillouin zone of the primitive cubic (FCC) structures to examine the electronic properties of bulk Pb/Te-based chalcogenides. The calculated band structures are shown in figures 2(a-d) and 3(a-d). Fig. 2 shows Electronic band structure of a)PbO, b)PbS, c)PbSe, and d) PbTe bulk chalcogenides. In the case of the PbO material (figure 2 (a)), the top of the valence band is around the L point, and the bottom of the conduction band is around the L point, implying that the PbO compound is a direct semiconductor with an energy band gap of 0.17 eV. Similarly, it is found that PbS, PbSe, and PbTe chalcogenides are direct band gap materials when we calculated the band structure along the symmetric L-L path. The obtained energy band gaps for PbS, PbSe, and PbTe compounds are 0.75, 0.57 and 0.85 eV, respectively. Fig. 3 shows Electronic band structure of a) SiTe, b) GeTe, c) PbTe, and d) SnTe bulk chalcogenides. The valence band intersects the Fermi energy in the case of SiTe and SnTe materials (Figs. 3a and d), showing its metallic character. Among this group, GeTe chalcogenide has the value of 0.5 eV energy gap. There are only slight differences in these energy gap values when compared with the earlier studies given in the references [72–75]. The density of electronic states (DOS) for XTe (X = Si, Ge, Sn and Pb) and PbY (Y = O, S, Se and Te) bulk chalcogenides are presented in figures 4(a-d) and 5(a-d). Fig. 4 shows density of electronic states of a) PbO, b) PbS, c) PbSe, and d) PbTe bulk chalcogenides. Fig. 5 shows Density of electronic states of a) SiTe, b) GeTe, c) PbTe, and d) SnTe bulk chalcogenides. It is seen from these figures that the number of electron states around the Fermi level is completely in accordance with the energy levels of the band structure of these materials from figures 2 and 3. From Figs. 5(a-d), it is also seen that the density of states around the Fermi band is crossing and it supports the metallic feature of SiTe chalcogenide. Also,

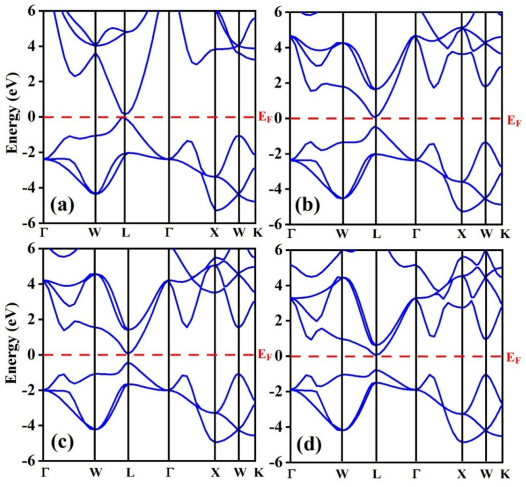

Figure 2. Electronic band structure of a) PbO, b) PbS, c) PbSe, and d) PbTe bulk chalcogenides.

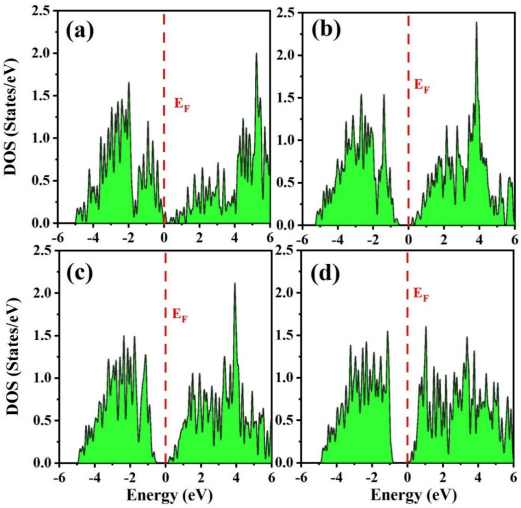

Figure 4. Density of electronic states of a) PbO, b) PbS, c) PbSe, and d) PbTe bulk chalcogenides.

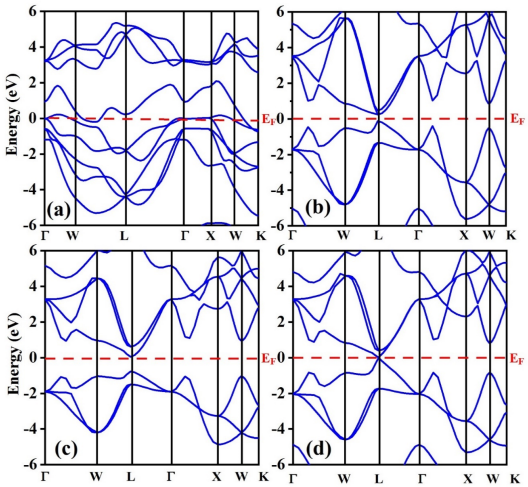

Figure 3. Electronic band structure of a) SiTe, b) GeTe, c) PbTe, and d) SnTe bulk chalcogenides.

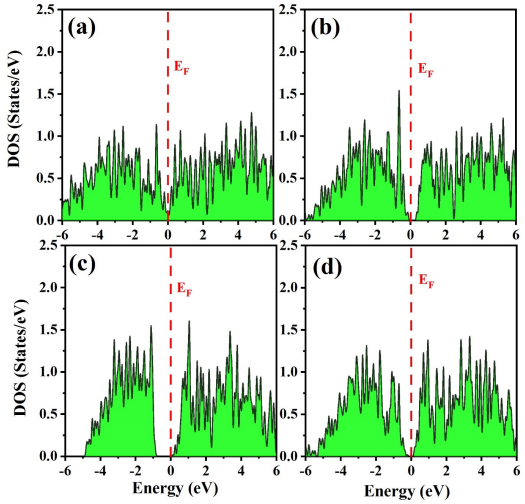

Figure 5. Density of electronic states of a) SiTe, b) GeTe, c) PbTe, and d) SnTe bulk chalcogenides.

PbO, PbS, PbSe, and PbTe nanolayers have energy gaps of 1.367, 0.706, 0.509 and 0.257 eV, respectively [76]. SiTe, GeTe, and SnTe nanolayers are characterized by the absence of energy gaps, rendering them as metallic materials [76]. Wherever there is a gap between the electronic bands, this gap is also observed in the density of states. Therefore, the results of DOS confirm the results of band structure.

3.3 Thermoelectric properties

In the analysis of Thermoelectric (TE) properties, key parameters include electrical conductivity (σ), thermal conductivity (κ) and Seebeck coefficient (S). To determine these coefficients, we utilized the Boltztrap computational code and semi-classical Boltzmann theory [77]. The TE parameters were calculated in the energy range of -2 to 2 eV and at temperatures of 300, 600, and 800 K.

Figures 6(a-d) and 7(a-d) depict the Seebeck coefficient (S) of bulk chalcogenides, XTe (X = Si, Ge, Sn and Pb) and PbY (Y = O, S, Se and Te), as a function of the chemical potential. Fig. 6 shows Seebeck coefficient of a) PbO, b) PbS, c) PbSe, and d) PbTe bulk chalcogenides. Fig. 7 shows Seebeck coefficient of a) SiTe, b) GeTe, c) PbTe and d) SnTe bulk chalcogenides. The most significant range of calculated S values is observed in the energy range of -0.5 to 0.5 eV, which is in close proximity to the Fermi level. As the energy moves away from the Fermi level, the S coefficient decreases and approaches zero. Furthermore, the figures demonstrate that the S coefficient decreases with increasing temperature. These findings indicate that these semiconductor compounds exhibit good thermal efficiency. The value of the Seebeck coefficient is positive over the measured temperature range, which shows p-type behavior, and it decreased with the increase of temperature. This value is negative in n-type behavior and decreased with increased of temperature. This opposite behavior is due to Seebeck effect, that temperature and S coefficient have opposite relation:

$$S = \frac{\Delta V}{\Delta T}$$

The chemical potential (μ) values provide information about the type of charge carriers present. When the chemical potential is positive, it indicates the presence of electron (n) carriers. Conversely, when the chemical potential is negative, it suggests the presence of hole (p) carriers. In all samples, there is a symmetrical behavior observed between holes and electrons for the Seebeck coefficient (S) around the Fermi surface. In the case of SiTe and SnTe chalcogenides, the increase in the density of electronic states around the Fermi level leads to the interference of conduction layer electrons with the Fermi surfaces. This interference results in a decrease in the S coefficient. Negative values of S correspond to n-type (electron) carriers, while positive values correspond to p-type (hole) carriers.

The highest value of the Seebeck coefficient among lead-based chalcogenides is observed in the PbTe compound. This can be attributed to its larger energy gap compared to other compounds. On the other hand, SiTe and SnTe compounds exhibit the lowest S coefficient values, likely due to their metallic behavior. Table 3 provides a comparison between the current study and previous research on S coefficient and energy gap values for Pb/Te-based chalcogenide nanolayers. The variation in the energy gap significantly affects the thermoelectric properties. The results of this comparison show that PbO, PbS and, PbSe nanolayers have a higher S coefficient than their bulk state. This shows that by decrease and changing the dimensions of the material from bulk to nanolayer, due to surface effects, the thermoelectric properties are improved.

In figures 8(a-d), and 9(a-d), the electrical conductivity (σ) of lead-based and tellurium-based chalcogenides is shown as a function of the chemical potential, respectively. Fig. 8 shows Electrical conductivity of a)PbO, b)PbS, c)PbSe, and, d)PbTe bulk chalcogenides. Fig. 9 shows Electrical conductivity of a) SiTe, b) GeTe, c) PbTe, and, d) SnTe bulk chalcogenides. Unlike the S diagrams, the electrical conductivity exhibits similar behavior at all temperatures. From these figures, it can be concluded that the values of σ increase with an increase in the chemical potential (μ) in

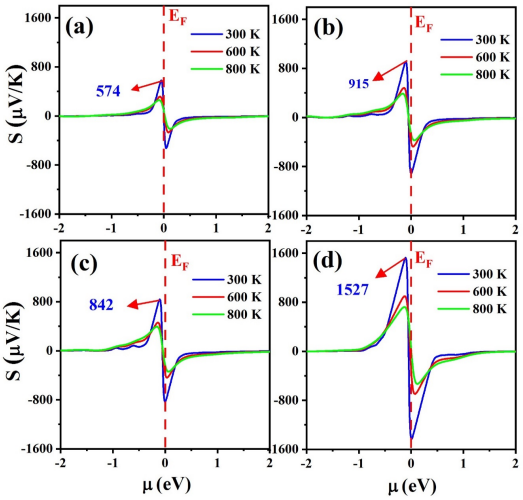

Figure 6. Seebeck coefficient of a)PbO, b)PbS, c)PbSe, and d)PbTe bulk chalcogenides in terms of chemical potential.

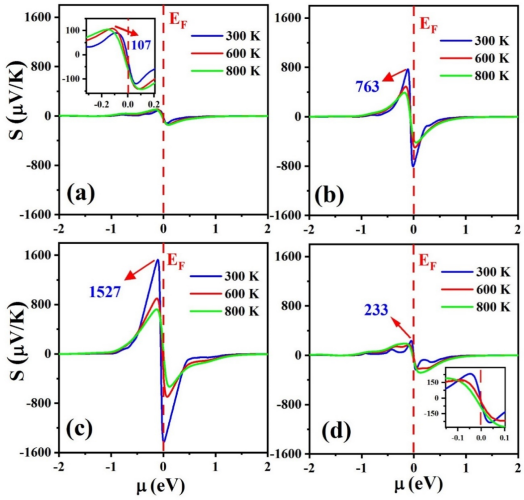

Figure 7. Seebeck coefficient of a)SiTe, b)GeTe, c)PbTe, and d)SnTe bulk chalcogenides in terms of chemical potential.

Table 3. Seebeck coefficient and band gap energy of Pb/Te-based chalcogenides.

Materials (bulk and nanolayers [57])	S (μV/κ)	E_g (eV)
PbO bulk-PbO nanolayer	574-2161	0.17-1.367
PbS bulk-Pbs nanolayer	915-1130	0.75-0.706
PbSe bulk-PbSe nanolayer	842-859	0.57-0.509
PbTe bulk-PbTe nanolayer	1527-424	0.85-0.257
SiTe bulk-SiTe nanolayer	107-33	metal-metal
GeTe bulk-GeTe nanolayer	763-634	0.5-metal
SnTe bulk-SnTe nanolayer	233-80	metal-metal

both the negative and positive regions. As μ increases, the density of charge carriers also increases, resulting in an increase in the conductivity of the material.

Figures 10(a-d), and 11(a-d) illustrate the thermal conductivity (κ) of lead-based and tellurium-based chalcogenides at temperatures of 300, 600 and, 800 K, within an energy range of -2 to 2 eV. Fig. 10 shows Thermal conductivity of a) PbO, b) PbS, c) PbSe, and d) PbTe bulk chalcogenides. Fig. 11 shows Thermal conductivity of a) SiTe, b) GeTe, c) PbTe, and, d) SnTe bulk chalcogenides. In all samples, the thermal conductivity increases with increasing temperature. This can be attributed to the increased density and vibrations of the charge carriers (electrons and holes) and an increase in the speed of dispersion. Electrical conductivity happens between the charges due to the transfer of energy in the form of voltage or current, whereas thermal conductivity

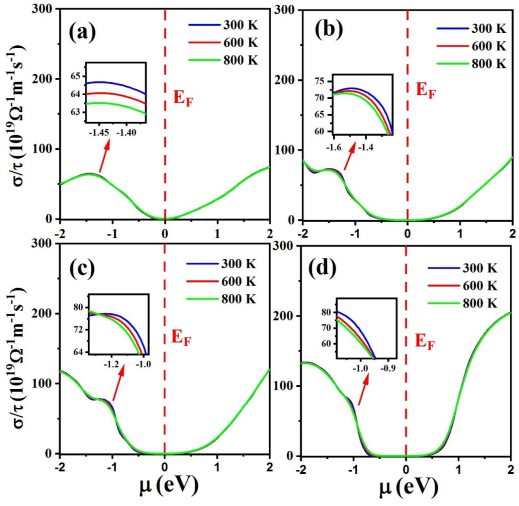

Figure 8. Electrical conductivity of a) PbO, b) PbS, c) PbSe, and d) PbTe bulk chalcogenides in terms of chemical potential.

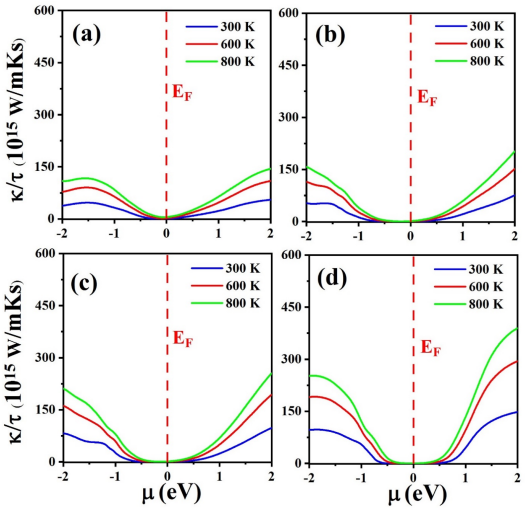

Figure 10. Thermal conductivity of a) PbO, b) PbS, c) PbSe, and d) PbTe bulk chalcogenides in terms of chemical potential.

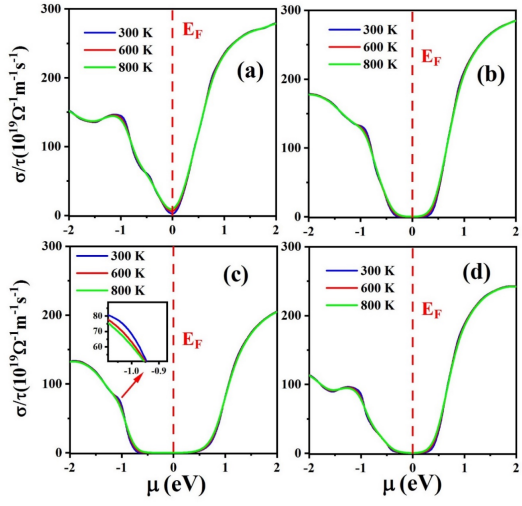

Figure 9. Electrical conductivity of a) SiTe, b) GeTe, c) PbTe, and d) SnTe bulk chalcogenides in terms of chemical potential.

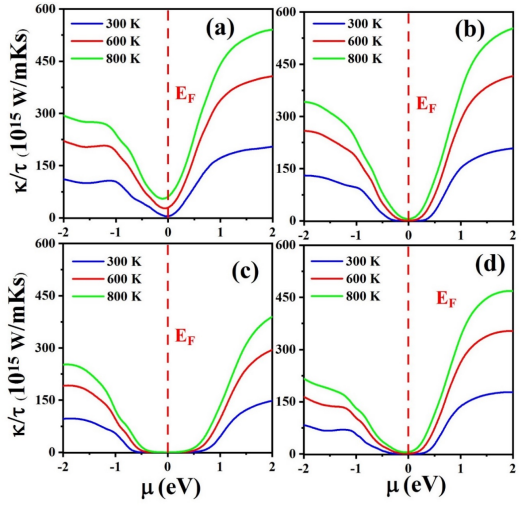

Figure 11. Thermal conductivity of a) SiTe, b) GeTe, c) PbTe, and d) SnTe bulk chalcogenides in terms of chemical potential.

is the transfer of energy between the molecules due to the impact of pressure called heat. In conductive structures, these values are higher than semi-conductive structures.
To enhance the TE properties, materials should have a high Seebeck coefficient (S) and electrical conductivity (σ), while maintaining a low thermal conductivity. According to [78], the optimal temperature to achieve the lowest thermal conductivity is 300 K. As observed in the figure, when the charge carriers are electrons, the thermal conductivity is higher compared to when the carriers are holes. According to equation 1, the higher Seebeck coefficient and electrical conductivity, and lower thermal conductivity, it causes the amount of ZT in the material to increase. According to the obtained values, among the bulk's materials, PbTe has the maximum ZT and among the nanolayers, PbO has the highest ZT value. Therefore, PbTe bulk and, PbO nanolayers show promising potential for thermoelectric applications.

3.4 Optical properties

In this section, the optical properties of bulk chalcogenides, specifically XTe (X = Si, Ge, Sn and, Pb) and PbY (Y =O, S, Se and, Te), have been investigated using the GGA approximation and epsilon.x code. These optical properties are obtained from the dielectric function, which is a complex quantity that describes the linear response of the material to electromagnetic radiation. The dielectric function consists of two parts: the real part (ε_1) and the imaginary part (ε_2). The response of materials to light is shown by dielectric function. This function should have two real and imaginary parts. The real part of this function shows light emission and the imaginary part shows light absorption in the material. When the imaginary value of the dielectric function of a material is higher, it is a better absorber and it is used in optical applications related to absorbers. Materials with higher real part are also used in light emission applications. The imaginary part of the dielectric function is calculated using the following formula from a theoretical perspective [79]:

$$\varepsilon_2(\omega) = \frac{4\pi^2 e^2}{m^2\omega^2}\sum_{i,f}\int \frac{2dk^{3^2}}{(2\pi)^3}|\langle ik|P_a|fk\rangle|^2\times$$

$$f_i^k(1-f_f^k)\delta(E_f^k - E_i^k - \omega) \qquad (2)$$

The relation mentioned represents the contribution of transitions between bands. In this relation, $|ik\rangle$ represents the state vector of the initial position, $|fk\rangle$ represents the state vector of the final position, $f_i{}^k$ is the Fermi distribution function for occupied states, and $f_f{}^k$ is the Fermi distribution function for unoccupied states. The ε_1 can be calculated using the ε_2 and the Kramers-Kronig relation [80–82]:

$$\varepsilon_1(\omega) = \delta_{\alpha\beta} + \frac{2}{\pi}Pr\int_0^\infty \frac{\omega' IM[\varepsilon_{\alpha\beta}(\omega')]}{\omega'^2 - \omega^2}d\omega' \qquad (3)$$

Figures 12(a, b), and 13(a, b), display the real part (ε_1) and imaginary part (ε_2) of the dielectric function for bulk chalcogenides, specifically XTe (X = Si, Ge, Sn and Pb) and, PbY (Y = O, S, Se and Te), as a function of energy. Fig. 12 shows the real part of the dielectric function for a) PbY (Y=O, S, Se and, Te) and b) XTe (X=Si, Ge, Sn and Pb) bulk chalcogenides. Fig. 13 shows the imaginary part of the dielectric function for a) PbY (Y=O, S, Se and, Te) and b) XTe (X=Si, Ge, Sn and, Pb) bulk chalcogenides. From the ε_2 data, it is evident that certain chalcogenide compounds possess an optical gap. The optical gap values for PbTe, PbSe, PbS, and, GeTe bulk materials are 0.8 eV, 1.8 eV, 2 eV and, 0.1 eV, respectively. Also, the optical gap of PbTe, PbSe, PbS, and, GeTe nanolayers is 0.76, 1.5, 1.85 and, 0.05 eV, respectively. The decrease in the optical gap of nanolayers compared to bulk indicates that electrons need less energy to be excited and create a phase transition in the nanolayer structure.
Figure 13 reveals that ε_2 becomes zero for PbO and PbTe materials at energies higher than 8 eV and for GeTe composition at energies higher than 4 eV. Additionally, the ε_2 values for PbS, PbSe and, SnTe chalcogenides become zero at energies higher than 5 eV and, for the SiTe compound at energies higher than 7 eV. In these energy ranges, these materials are not transparent; instead, they appear dark and do not allow penetration of electromagnetic waves. Consequently, they can be utilized as absorbent materials [86].
In the energy range of 0 to 4 eV, the ε_2 exhibits an initial increase followed by a decrease. This behavior indicates the occurrence of inter-band transitions in these compounds. Figure 12 reveals that the ε_1 is negative in the range of 2 to 5 eV, indicating that waves do not propagate in this energy region. The surfaces of these compounds can be

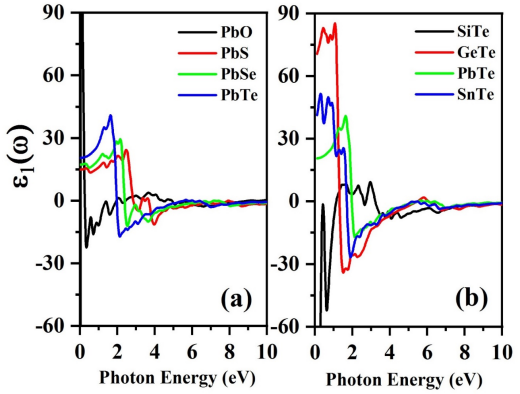

Figure 12. The real part of the dielectric function for a)PbY (Y=O, S, Se, and Te) and b) XTe (X=Si, Ge, Sn, and Pb) bulk chalcogenides.

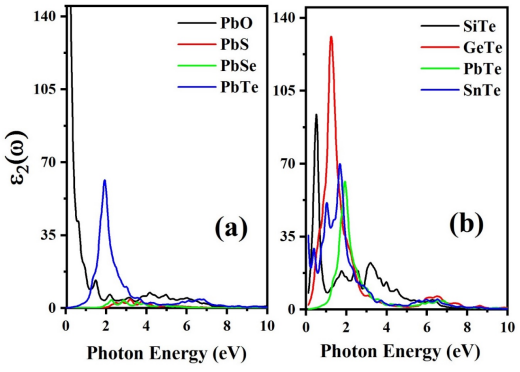

Figure 13. The imaginary part of the dielectric function for a) PbY (Y=O, S, Se and Te) and b) XTe (X=Si, Ge, Sn and Pb) bulk chalcogenides.

utilized as magnetic filters to absorb waves within this energy range. Furthermore, the static dielectric constant (ε_1 at zero energy) for PbTe, PbSe, PbS, GeTe, and, SnTe compounds is approximately 20, 18, 17, 79, and 43, respectively. The static refractive index (n_0) of these materials can be obtained by taking the square root of the static dielectric constant. Specifically, the values of n_0 are 4.47, 4.24, 4.12, 8.88, and 6.55 for PbTe, PbSe, PbS, GeTe, and, SnTe bulk chalcogenides, respectively. The refractive index values for PbTe, PbSe, PbS, GeTe, and, SnTe nanolayers are 1.58, 1.51, 1.54, 2.23, and, 1.87, respectively. The decrease in the refractive index of nanolayers compared to bulks indicates more absorption of light by nanolayers.

Table 4 presents the optical gap and n_0 values from this study as well as other research works. To calculate the reflectivity (R) and absorption coefficient (A), the following relations are employed:

$$R = |\frac{(n(\omega)-1)^2 + k(\omega)^2}{(n(\omega)+1)^2 + k(\omega)^2}| \quad (4)$$

$$A(\omega) = \frac{2k(\omega)E}{\hbar c} \quad (5)$$

In the given formula, n and k represent the real and imaginary parts of the refractive index (or optical coefficients). These coefficients can be expressed in terms of the real and imaginary parts of the dielectric function as follows:

$$n(\omega) = \sqrt{1/2(\sqrt{\varepsilon_1(\omega)^2 + \varepsilon_2(\omega)^2} + \varepsilon_1(\omega))} \quad (6)$$

$$k(\omega) = \sqrt{1/2(\sqrt{\varepsilon_1(\omega)^2 + \varepsilon_2(\omega)^2} - \varepsilon_1(\omega))} \quad (7)$$

When light is applied to a material, part of it is absorbed, another part is transmitted and the final part is reflected. The resistance of a material to the transmitted of light is called optical resistance. Figures 14(a, b), and 15(a, b) depict the graphs of the absorption and reflectance coefficients as a function of energy for these materials, considering the vertical direction of the electric field. Fig. 14 shows the optical absorption of a) PbY (Y=O, S, Se, and, Te) and b) XTe (X=Si, Ge, Sn, and Pb) bulk chalcogenides. Fig. 15 shows the optical reflectivity of a) PbY (Y=O, S, Se, and, Te) and b) XTe (X=Si, Ge, Sn, and, Pb) bulk chalcogenides. Upon careful examination of these figures, it is evident that the reflection is minimal at low energies and the variations in these functions exhibit a direct relationship with changes in energy. Optical Absorption Edge' refers to the photon energy level at which the absorption behavior of semiconductors changes, characterized by an optical gap. It can be analyzed using the Tauc formula above the optical gap and the Urbach formula below it. A higher absorption edge in a material corresponds to a larger optical gap, indicating improved absorption properties in the visible region. The findings of this study reveal that PbS exhibits the largest optical gap among nanolayers, while GeTe shows the largest optical gap in bulk form.

4. Conclusion

In this article, the electronic, structural, thermoelectric and optical properties of bulk and nanolayers chalcogenides, XTe (X = Si, Ge, Sn, and, Pb) and PbY (Y = O, S, Se, and, Te) were investigated using the DFT and the semiclassical Boltzmann method. The calculations conducted in this research demonstrated that these materials exhibit significant potential in thermoelectric applications, primarily due to their high S and σ coefficients. The electronic band structure analysis revealed that PbO, PbS, PbSe, PbTe, and, GeTe compounds are direct band-gap

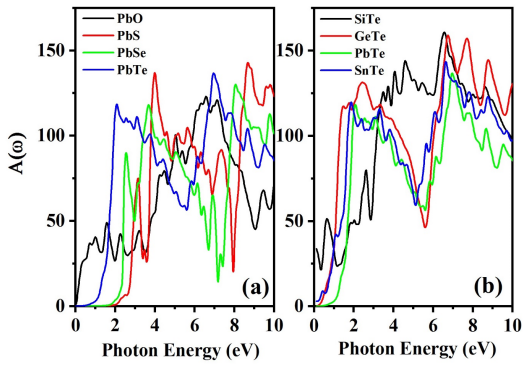

Figure 14. The optical absorption of a) PbY (Y=O, S, Se, and Te) and b) XTe (X=Si, Ge, Sn, and Pb) bulk chalcogenides.

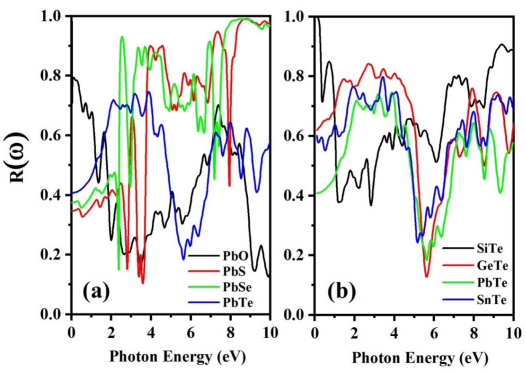

Figure 15. The optical reflectivity of a) PbY (Y=O, S, Se, and Te) and b) XTe (X=Si, Ge, Sn, and Pb) bulk chalcogenides.

Table 4. The optical gap and n_0 of Pb/Te-based chalcogenides.

Materials	n_0	Optical gap (eV)	Other works
PbTe	4.47	0.8	5.5-0.81 [83]
PbSe	4.24	1.8	4.25-1.5 [84]
PbS	4.12	2.0	4.1-1.8 [84]
Gete	8.88	0.1	6.2-0.07 [85]
SnTe	6.55	0.01	6.4-0.03 [85]

semiconductors. Additionally, the valence bands of SiTe and, SnTe compounds slightly intersect the Fermi energy level, indicating the metallic nature of this particular group of materials. In the nanolayer structure, the energy gap was changed, the GeTe material changed from a semiconductor to a metal. The PbTe compound exhibits the highest Seebeck coefficient at 300 K indicating its superior thermoelectric properties compared to other materials in this group. Also, the thermoelectric properties of some materials in the nanolayer state were significantly improved. The most promising potential for thermoelectric applications is PbTe bulk and PbO nanolayer. Furthermore, the optical analysis revealed that the imaginary part of the dielectric function (ε_2) initially increases and then decreases in the energy range of 0-4 eV, indicating the occurrence of inter-band transitions in these compounds. PbS material has the lowest refractive index and the highest optical gap in both the bulk and the nanolayer structure, making it a suitable option for optoelectronic applications.

Acknowledgment:
The computing resources utilized in this research were supported by the Dena High-Performance Computing (HPC) facility at Yasouj University.

Authors contributions
Authors have contributed equally in preparing and writing the manuscript.

Availability of data and materials
The data that support the findings of this study are available from the corresponding author, [SJN], upon reasonable request.

Conflict of interests
The authors declare that they have no known competing financial interests or personal relationships that could have appeared to influence the work reported in this paper.

References

[1] E. Gapp and P. Pfeifer. Membrane reactors for hydrogen production from renewable energy sources. *Current Opinion in Green and Sustainable Chemistry*, 41:100800, 2023.
DOI: https://doi.org/10.1016/j.cogsc.2023.100800.

[2] H. Q. Pham, T. Q. PhamH, Q. Huynh, and T. T. Huynh. Single-atom iridium-based catalysts: synthesis strategies and electro (photo)-catalytic applications for renewable energy conversion and storage. *Coordination Chemistry Reviews*, 486:215143, 2023.
DOI: https://doi.org/10.1016/j.ccr.2023.215143.

[3] Y. Y. Feng, Y. Q. Chen, Z. Wang, and J. Wei. Synthesis of mesoporous carbon materials from renewable plant polyphenols for environmental and energy applications. *New Carbon Materials*, 37: 196–222, 2022.
DOI: https://doi.org/10.1016/S1872-5805(22)60577-8.

[4] M. S. Sadjadi, B. Sadeghi, and K. Zare. Natural bond orbital (nbo) population analysis of cyclic thionylphosphazenes, [nsox (npcl2)2]; x=f (1), x=cl (2). *Journal of Molecular Structure: THEOCHEM*, 817:27–33, 2007.
DOI: https://doi.org/10.1016/j.theochem.2007.04.015.

[5] M. Hamid Elsheikh, D. A. Shnawah, M. F. M. Sabri, S. B. M. Said, M. Haji Hassan, M. B. Ali Bashir, and M. Mohamad. A review on thermoelectric renewable energy: Principle parameters that affect their performance. *Renewable and Sustainable Energy Reviews*, 30: 337–355, 2014.
DOI: https://doi.org/10.1016/j.rser.2013.10.027.

[6] A. V. da Rosa and J. C. Ordonez. Chapter 5 - thermoelectricity, in: da rosaa.v., ordonez j.c. (eds.) fundamentals of renewable energy processes (fourth edition),. *Academic Press, Oxford*, pages 187–247, 2022.

[7] M. Zhang, Y. Tian, H. Xie, Z. Wu, and Y. Wang. Influence of thomson effect on thethermoelectric generator. *International Journal of Heat and Mass Transfer*, 137:1183–1190, 2019.
DOI: https://doi.org/10.1016/j.ijheatmasstransfer.2019.03.155.

[8] Z. Liu, S. Liu, J. Zhao, Y. Yue, Q. Xu, and F. Yang. A transient heat flux sensor based on the transverse seebeck effect of single crystal bi_2te_3. *Measurement*, 198:111419, 2022.
DOI: https://doi.org/10.2139/ssrn.4034690.

[9] G. J. Snyder and A. H. Snyder. Figure of merit zt of a thermoelectric device defined from materials properties. *Energy and Environmental Science*, 10(2280-2283), 2017.
DOI: https://doi.org/10.1039/C7EE02007D.

[10] T. Jiao, C. You, N. Tian, L. Ma, Z. Duan, F. Yan, P. Ren, and G. Zhao. Achieving high breakdown strength and figure of merit of $ba_{0.6}sr_{0.4}tio_3$ films through coating a $y_3fe_5o_{12}$ layer. *Journal of the European Ceramic Society*, 42:4926–4933, 2022.
DOI: https://doi.org/10.1016/j.jeurceramsoc.2022.05.038.

[11] D. Sekyi-Arthur, M. Egblewogbe, S. Y. Mensah, N. G. Mensah, K. W. Adu, K. A. Dompreh, R. Edziah, and S. Atarah. Giant thermoelectric figure of merit in fluorine-doped single walled-carbon nanotubes. *Physica E: Low-dimensional Systems and Nanostructures.*, 142:115292, 2022.
DOI: https://doi.org/10.1016/j.physe.2022.115292.

[12] A. Abdelakader, B. Ahmed, M. Noureddine, B. Mokhtar, Z. Abdelhalim, and M. Omar. Theoretical investigations of electronic, thermodynamic and thermoelectric properties of filled skutterudites $thfe_4p_{12}$ and $cefe_4p_{12}$ using dft calculations. *Solid State Communications*, 380:115435, 2022.
DOI: https://doi.org/10.1016/j.ssc.2024.115435.

[13] D. Allali, B. Abdelmadjid, S. E. Saber, D. Bahri, F. Zerarga, and R. Amari. A first-principles investigation on the structural, electronic and optical characteristics of tetragonal compounds xago (x = li, na, k, rb). *Computational Condensed Matter*, 38:e00876, 2024.
DOI: https://doi.org/10.1016/j.cocom.2023.e00876.

[14] H. Allaf, M. Radjai, D. Allali, A. Bouhemadou, S. S. Essaoud, and S. Bin-Omran. Ab initio predictions of pressure-dependent structural, elastic, and thermodynamic properties of $calix_3$ (x = cl, br, and i) halide perovskites. *Computational Condensed Matter*, 37:e00850, 2023.
DOI: https://doi.org/10.1016/j.cocom.2023.e00850.

[15] D. Allali, R. Amari, A. Bouhemadou, A. Boukhari, B. Deghfel, and S. S. Essaoud. Ab initio investigation of structural, elastic, and thermodynamic characteristics of tetragonal xago compounds (x = li, na, k, rb). *Physica Scripta*, 98(11):115905, 2023.
DOI: https://doi.org/10.1088/1402-4896/acfbfe.

[16] J. I. Al-Hawarin, A-A. Abu-Yamin, AA-AA Abu-Saleh, I. A. Saraireh, M. H. Almatarneh, and M. Hasan. Synthesis, characterization, and dft calculations of a new sulfamethoxazole schiff base and its metal complexes. *Materials*, 16(14):5160, 2023.

[17] R. Samia, A. Yahia, B. Ahmed, B. Mokhtar, M. Noureddine, and L. Mohamed. Electronic, elastic and piezoelectric properties calculations of perovskites materials type $bixo_3$(x = al, sc): Dft and dfpt investigations. *Chemical Physics*, 573:111998, 2023.
DOI: https://doi.org/10.1016/j.chemphys.2023.111998.

[18] B. Tahir, A. Bouhemadou, S. Bin-Omran, R. Khenata, Y. Al-Douri, and N. Guechi. Ab initio predictions of the structural, electronic, optical, elastic, and thermoelectric properties of quasi-two-dimensional bafznp. *Computational Condensed Matter*, 35:e00809, 2023.
DOI: https://doi.org/10.1016/j.cocom.2023.e00809.

[19] F. O. Gaid, F. Z. Boufadi, N. Tayebi, M. Ameri, A. Mentefa, and L. Bellagoun. Theoretical investigation of structural, electronic, elastic, magnetic, thermodynamic, and thermoelectric properties of ru_2mnnb heusler alloy: Fp-lmto method. *Emergent Materials*, 5(4): 1065–73, 2022.
DOI: https://doi.org/10.1007/s42247-021-00229-y.

[20] A. Saim, F. Belkharroubi, F. Z. Boufadi, I. Ameri, L. F. Blaha, and A. Tebboune. Investigation of the structural, elastic, electronic, and optical properties of half-heusler camgz (z = c, si, ge, sn, pb) compounds. *Journal of Electronic Materials*, 51(7):4014–28, 2022.
DOI: https://doi.org/10.1007/s11664-022-09659-8.

[21] C. Lertsatitthanakorn. Electrical performance analysis and economic evaluation of combined biomass cook stove thermoelectric (bite) generator. *Bioresource Technology*, 98:1670–1674, 2007.
DOI: https://doi.org/10.1016/j.biortech.2006.05.048.

[22] J. Jang, B. K. Koo, M. S. Kim, and J. E. Lee. Microstructure change and thermal conductivity reduction in p-type bi–sb–te thermoelectric materials using a metal fatty acid as process control agent. *Applied Surface Science*, 611:155643, 2023.
DOI: https://doi.org/10.2139/ssrn.422939.

[23] V. Pal, B. Kumar, M. K. Paek, C. S. Tiwary, and M. Paliwal. Microstructure design in bi-ga-te system using a combination of thermodynamic calculations and experiments for potential thermoelectric material. *Materials Chemistry and Physics*, 297:127366, 2023.
DOI: https://doi.org/10.1016/j.matchemphys.2023.127366.

[24] W. Cao, J. Gao, and J. Zhang. Study on output characteristics of hot-pressed bi_2te_3 based thermoelectric generator. *Procedia Engineering*, 27:144–150, 2012.
DOI: https://doi.org/10.1016/j.proeng.2011.12.436.

[25] K. A.Morgan, I. Zeimpekis, Z. Feng, and D. Hewak. Enhancing thermoelectric properties of bismuth telluride and germanium telluride thin films for wearable energy harvesting. *Thin Solid Films*, 741: 139015, 2022.
DOI: https://doi.org/10.1016/j.tsf.2021.139015.

[26] M. Shtern, A. Sherchenkov, Y. Shtern, N. Borgardt, M. Rogachev, A. Yakubov, A. Babich, D. Pepelyaev, I. Voloshchuk, Y. Zaytseva, S. Pereverzeva, A. Gerasimenko, D. Potapov, and D. Murashko. Mechanical properties and thermal stability of nanostructured thermoelectric materials on the basis of pbte and gete. *journal of Alloys and Compounds*, 946:169364, 2023.
DOI: https://doi.org/10.1016/j.jallcom.2023.169364.

[27] O. Khshanovska, T. Parashchuk, and I. Horichok. Estimating the upper limit of the thermoelectric figure of merit in n- and p-type pbte. *Materials Science in Semiconductor Processing*, 160:107428, 2023.
DOI: https://doi.org/10.1016/j.mssp.2023.107428.

[28] F. Lv, Y. Zhong, X. Zhao, X. An, L. Lin, D. Ren, B. Liu, and R. Ang. High-performance thermoelectrics of p-type pbte via synergistic regulation of band and microstructure engineering. *Materials Today Physics*, 34:101061, 2023.
DOI: https://doi.org/10.1016/j.mtphys.2023.101061.

[29] X. Li, W. Xu, Y. Wang, X. Zhang, Z. Hui, H. Zhang, S. Wageh, OA. Al-Hartomy, and AG. Al-Sehemi. Optical-intensity modulators with pbte thermoelectric nanopowders for ultrafast photonics. *Applied Materials Today*, 28:101546, 2022.
DOI: https://doi.org/10.1016/j.apmt.2022.101546.

[30] Z. Fan, J. Liang, J. L. Chen, Y. Peng, H. Lai, J. Nong, C. Liu, W. Ding, and L. Miao. Realizing high thermoelectric performance for p-type sige in medium temperature region via tac compositing. *Journal of Materiomics*, 9:984–991, 2023.
DOI: https://doi.org/10.1016/j.jmat.2023.03.004.

[31] S. J. Hong, H. Chun, C. Kwon, and B. Han. n-type thermoelectric properties of a hexagonal sige polymorph superior to a cubic sige. *Journal of Alloys and Compounds*, 874:160007, 2021.
DOI: https://doi.org/10.1016/j.jallcom.2021.16000.

[32] Y. Li, J. Li, J. Du, J. Han, Q. Xiang, and C. Zhang. Influence of fast neutron and gamma irradiation on the thermoelectric properties of n-type and p-type sige alloy. *Journal of Nuclear Materials*, 528: 151856, 2020.
DOI: https://doi.org/10.1016/j.jnucmat.2019.151856.

[33] K. Xie and M. C. Gupta. Thermoelectric properties of sige thin films prepared by laser sintering of nanograin powders. *Journal of Alloys and Compounds*, 820:153182, 2020.
DOI: https://doi.org/10.1016/j.jallcom.2019.153182.

[34] R. Murugasami, P. Vivekanandhan, S. Kumaran, R. Suresh Kumar, and T. John Tharakan. Synergetic enhancement of thermoelectric and mechanical properties of n-type sige-p alloy through solid state synthesis and spark plasma sintering. *Materials Research Bulletin*, 118:110483, 2019.
DOI: https://doi.org/10.1016/j.materresbull.2019.05.008.

[35] A. Alashkar and A. H. Alami. Overview of thermoelectric materials, in: A.-g. olabi (ed.). *Encyclopedia of Smart Materials, Elsevier, Oxford*, pages 319–325, 2022.

[36] E. Pakizeh and M. Mohammadi. Structural, electronic, magnetic and thermoelectric properties of pseudobrookite-type fe2-xti1+ xo5 (x= 0, 0.5 and 1) compounds: Dft+ u approaches. *Journal of Physics and Chemistry of Solids*, 149:109802, 2021.
DOI: https://doi.org/10.1016/j.jpcs.2020.109802.

[37] K. B. Masood, N. Jain, P. Kumar, M. A. Malik, and J. Singh. Nanostructured thermoelectric materials, in: R. kumar, r. singh (eds.). *Thermoelectricity and Advanced Thermoelectric Materials, Woodhead Publishing*, pages 261–311.
DOI: https://doi.org/2021.

[38] Y.Nonoguchi. Thermoelectric materials and devices based on carbon nanotubes, in: R. funahashi (ed.). *Thermoelectric Energy Conversion, Woodhead Publishing*, 2.(14):367–373, 2021.

[39] M. Mohammadi and E. Pakizeh. Electronic structure, optical properties, and potential applications of n-bn/ws2 (n = 1 to 4) heterostructures. *Journal of Electronic Materials*, 50:4696–4704, 2021.
DOI: https://doi.org/10.1007/s11664-021-09015-2.

[40] Q. Wei, M. Mukaida, K. Kirihara, and T. Ishida. Thermoelectric materials-based on organic semiconductors, in: R. funahashi (ed.). *Thermoelectric Energy Conversion, Woodhead Publishing*, 2(12): 333–345, 2021.

[41] E. Pakizeh and R. Darvishi. Investigation of adsorption of copper, zinc and cadmium metals by polymeric coagulant polyaluminum chloride based on density functional theory. *Advanced Materials and New Coatings*, 10:2740–2747, 2021.
DOI: https://doi.org/2021.10.37.5.

[42] H. Wang and C. Yu. Organic thermoelectric materials and devices, in: R. funahashi (ed.). *Thermoelectric Energy Conversion, Woodhead Publishing*, 2(13):347–365, 2021.

[43] E. Pakizeh, J. Jalilian, and M. Mohammadi. Electronic, optical and thermoelectric properties of fe_2zrp compound determined via first-principles calculations. *RSC Advances*, 9:25900–25911, 2019.
DOI: https://doi.org/10.1039/C9RA04736K.

[44] X. Chen, W. Dai, T. Wu, W. Luo, J. Yang, W. Jiang, and L. Wang. Thin film thermoelectric materials: classification, characterization, and potential for wearable applications. *Coatings*, 8:244, 2018.
DOI: https://doi.org/10.3390/coatings8070244.

[45] Y. Pan, U. Aydemir, F. H. Sun, C. F. Wu, T. C. Chasapis, G. J. Snyder, and J. F. Li. Self-tuning n-type bi_2(te,se)3/sic termoelectric nanocomposites to realize high performances up to 300 ^{O}c. *Advanced Science*, 4:1700259, 2017.
DOI: https://doi.org/10.1002/advs.201700259.

[46] Z. Soleimani, S. Zoras, B. Ceranic, S. Shahzad, and Y. Cui. A review on recent developments of thermoelectric materials for room-temperature applications. *Sustainable Energy Technologies and Assessments*, 37:100604, 2020.
DOI: https://doi.org/10.1016/j.seta.2019.100604.

[47] J. P. Heremans, V. Jovovic, E. S. Toberer, A. Saramat, K. Kurosaki, A. Charoenphakdee, S. Yamanaka, and G. J. Snyder. Enhancement of thermoelectric efficiency in pbte by distortion of the electronic density of states. *Science*, 321:554–557, 2008.
DOI: https://doi.org/10.1126/science.1159725.

[48] Y. Pei, X. Shi, A. LaLonde, H. Wang, L. Chen, and G. J. Snyder. Convergence of electronic bands for high performance bulk thermoelectrics. *Nature*, 473:66–69, 2011.
DOI: https://doi.org/10.1038/nature09996.

[49] Y. Pei, A. LaLonde, S. Iwanaga, and G. J. Snyder. High thermoelectric figure of merit in heavy hole dominated pbte. *Energy and Environmental Science*, 4:2085–2089, 2011.
DOI: https://doi.org/10.1039/c0ee00456a.

[50] P. Mishra, D. Singh, Y. Sonvane, and R. Ahuja. Two-dimensional boron monochalcogenide monolayer for thermoelectric materiall. *Sustainable Energy and Fuels*, 4:2363–2369, 2020.
DOI: https://doi.org/10.1039/D0SE00004C.

[51] R. Gupta, N. Kumar, P. Kaur, and C. Bera. Theoretical model for predicting thermoelectric properties of tin chalcogenides. *Physical Chemistry Chemical Physics*, 22:18989–19008, 2020.
DOI: https://doi.org/10.1039/D0CP03117H.

[52] H. Salehi, N. Shahtahmasebi, S. M. Hosseini, N. Shahtahmasebi, and S. M. Hosseini. Calculation of optical properties and electronic structure of batio$_3$. *Iranian Journal of Physics Research*, 5:47–52, 2019.

[53] S. Azam, M. Irfan, Z. Abbas, M. Rani, T. Saleem, A. Younus, N. Akhtarand B. Liaqat, M. Shabbir, and A. G. Al-Sehemi. Dft study of the electronic and optical properties of ternary chalcogenides alx$_2$te$_4$. *Materials Research Express*, 6:116314, 2019.
DOI: https://doi.org/10.1088/2053-1591/ab4b81.

[54] T. Mathew, K. S. Rahul, S. Joseph, and V. Mathew. Density functional study of structural, electronic and optical properties of quasi-one-dimensional compounds batix3 (x=s, se). *Superlattices and Microstructures*, 153:106859, 2021.
DOI: https://doi.org/10.1016/j.spmi.2021.106859.

[55] S. Goumri-Said, M. A. Shah, S. Azam, M. Irfan, and M. B. Kanoun. Investigation of electronic and optical properties of the ternary chalcogenides for optoelectronic applications: A tb-mbj dft study. *Current Applied Physics*, 49:151–157, 2023.
DOI: https://doi.org/10.1016/j.cap.2023.02.021.

[56] N. Pandit, R. Singh, A. Kumar, T. K. Joshi, A. Shukla, and U. Rani. Physical properties and power conversion efficiency of srzrx$_3$ (x=s and se) chalcogenide perovskite solar cell. *Modern Physics Letters B*, page 2450345, .
DOI: https://doi.org/10.1142/s0217984924503457.

[57] N. Pandit, A. Dubey, T. K. Joshi, A. Shukla, U. Rani, and P. K. Kamlesh. Effect of anion (s-2 and se-2) replacement on photovoltaic properties in transition metal (ba-barium) chalcogenide perovskites. *International Journal of Modern Physics B*, page 2550059, .
DOI: https://doi.org/10.1142/s0217979225500596.

[58] J. K. Bairwa, P. K. Kamlesh, U. Rani, R. Singh, R. Gupta, and S. Kumari. Highly efficient and stable ra$_2$lanbo$_6$ double perovskite for energy conversion device applications. *Materials science for energy technologies*, 7:61–72, 2024.
DOI: https://doi.org/10.1016/j.mset.2023.07.005.

[59] M. Rani, P. K. Kamlesh, S. Kumawat, Anuradha, U. Rani, and G. Arora. Rare earth-based oxides double perovskites a2nimno6 (a= la and gd): Applications in magneto-caloric, photo-catalytic and thermoelectric devices. *Physica B: Condensed Matter*, 680:415645, 2024.
DOI: https://doi.org/10.1016/j.physb.2023.415645.

[60] J. K. Bairwa, M. Rani, P. K. Kamlesh, R. Singh, U. Rani, and S. Al-Qaisi. Modeling and simulation of multifaceted properties of x$_2$naio$_6$ (x=ca and sr) double perovskite oxides for advanced technological applications. *Journal of Molecular Modeling*, 29(12):379, 2023.
DOI: https://doi.org/10.1007/s00894-023-05786-z.

[61] M. Rani, P. K. Kamlesh, S. Kumawat, Anuradha, U. Rani, and G. Arora. Ab-initio calculations of structural, optoelectronic, thermoelectric, and thermodynamic properties of mixed-halide perovskites rbpbbr$_3$-xix (x = 0 to 3):applicable in renewable energy devices. *ECS Journal of Solid State Science and Technology*, 12(8):083006, 2023.
DOI: https://doi.org/10.1149/2162-8777/acec9c.

[62] A. Dubey, N. Pandit, R. Singh, T. K. Joshi, B. L. Choudhary, and P. K. Kamlesh. Lead-free alternative cation (ethylammonium) in organometallic perovskites for thermoelectric applications. *Journal of Molecular Modeling*, 30(3):77, 2024.
DOI: https://doi.org/10.1007/s00894-024-05867-7.

[63] S. Kumari, U. Rani, M. Rani, R. Singh, P. K. Kamlesh, and S. Kumari. Computational investigation of the fundamental physical properties of lead-free halide double perovskite rb$_2$nacox$_6$ (x = cl, br, and i) materials: Potential prospects for sustainable energy. *Modern Physics Letters B*, page 2450323.
DOI: https://doi.org/10.1142/s0217984924503238.

[64] P. Giannozzi, S. Baroni, N. Bonini, M. Calandra, R. Car, C. Cavazzoni, D. Ceresoli, G. L. Chiarotti, M. Cococcioni, I. Dabo, A. Dal Corso, S. de Gironcoli, S. Fabris, G. Fratesi, R. Gebauer, U. Gerstmann, C. Gougoussis, A. Kokalj, M. Lazzeri, L. Martin-Samos, N. Marzari, F. Mauri, R. Mazzarello, S. Paolini, A. Pasquarello, L. Paulatto, C. Sbraccia, S. Scandolo, G. Sclauzero, A. P. Seitsonen, A. Smogunov, P. Umari, and R. M. Wentzcovitch. Quantum espresso: a modular and open-source software project for quantum simulations of materials. *Journal of Physics: Condensed Matter*, 21:395502, 2009.
DOI: https://doi.org/10.1088/0953-8984/21/39/395502.

[65] C. Ribaldone, D. Dragoni, and M. Bernasconi. A first-principles study of the switching mechanism in gete/insbte superlattices. *Nanoscale Advances*, 2(11):5209–18, 2022.
DOI: https://doi.org/10.1039/D0NA00577K.

[66] P. Bauer Pereira, I. Sergueev, S. Gorsse, J. Dadda, E. Muller, and RP. Hermann. Lattice dynamics and structure of gete, snte and pbte. *physica status solidi (b)*, 250(7):1300–7, 2013.
DOI: https://doi.org/10.1002/pssb.201248412.

[67] S. Miotkowska, E. Dynowskaand I. Miotkowski, A. Szczerbakow, B. Witkowska, and J. Kachniarz. The lattice constants of ternary and quaternary alloys in the pbte–snte–mnte system. *Journal of Crystal Growth*, 200(3):483–9, 1999.
DOI: https://doi.org/10.1016/S0022-0248(99)00038-X.

[68] K. S. Syed Ali, R. Saravanan, S. Israel, and R. K. Rajaram. Electron density distribution and bonding in znse and pbse using maximum entropy method (mem). *Bulletin of Materials Science*, 29(2):107–14, 2006.
DOI: https://doi.org/10.1007/BF02704601.

[69] H. Dehdashti Jahromi. Optical and electronic properties of lead sulfide spherical nano particle. *Optik*, 231:166503, 2021.
DOI: https://doi.org/10.1016/j.ijleo.2021.166503.

[70] J. Berashevich, O. Semeniuk, O. Rubel, J. A. Rowlands, and A. Reznik. Lead monoxide α-pbo: electronic properties and point defect formation. *Journal of Physics: Condensed Matter*, 25(7): 075803, 2013.
DOI: https://doi.org/10.1088/0953-8984/25/7/075803.

[71] J. P. Perdew, K. Burke, and M. Ernzerhof. Generalized gradient approximation made simple. *Physical Review Letters*, 77:3865–3868, 1996.
DOI: https://doi.org/10.1103/PhysRevLett.77.3865.

[72] J. O. Akinlami, M. O. Omeike, J. A. Akindiilete, and L. O. Abdulfatai. Electronic properties and the phonon band structure of pbte. *Computational Condensed Matter*, 15:90–94, 2018.
DOI: https://doi.org/10.1016/j.cocom.2017.10.005.

[73] Picozzi S. Ferroelectric rashba semiconductors as a novel class of multifunctional materials. *Frontiers in Physics*, 2:1–9, 2014.
DOI: https://doi.org/10.3389/fphy.2014.00010.

[74] L. Shoukat, M. Butt, S. Saleem, Z. Elqahtani, S. Aldaghfag, M. Ishfaq, M. Yaseen, E. Yousef, and H. Hegazy. Tuned physical characteristics of pbse binary compound: a dft study. *Journal of Ovonic Research*, 18:185–649, 2022.
DOI: https://doi.org/10.15251/JOR.2022.185.649.

[75] K. M. Wong, S. M. Alay e Abbas, Y., A. Shaukat, and Y. Lei. Dft+ u study of the structural and electronic properties of the ferromagnetic and antiferromagnetic ordering in the pbs-based ternary alloys pb1-xeuxs (x= 0.25, 0.50, 0.75 and 1). *Solid State Sciences*, 18:24–35, 2013.
DOI: https://doi.org/10.1016/j.solidstatesciences.2012.12.008.

[76] K. Rajabi, E. Pakizeh, H. Tashakori, and F. Taghizadeh-Farahmand. First principle analysis of the structural, electrical and thermoelectric properties of yte (ysi, pb, sn, ge) and pbx (x= o, s, se, te) nano-layers. *Solid State Communications*, 359:115023, 2023.
DOI: https://doi.org/10.1016/j.ssc.2022.115023.

[77] G. K. H. Madsen and D. J. Singh. Boltztrap. a code for calculating band-structure dependent quantities. *Computer Physics Communications*, 175:67–71, 2006.
DOI: https://doi.org/10.1016/j.cpc.2006.03.007.

[78] G. J. Snyder and E. S. Toberer. Complex thermoelectric materials. *Nature Materials*, 7:105–114, 2008.
DOI: https://doi.org/10.1038/nmat2090.

[79] C. Ambrosch-Draxl and J. O. Sofo. Linear optical properties of solids within the full-potential linearized augmented planewave method. *Computer physics communications*, 175:1–14, 2006.
DOI: https://doi.org/10.1016/j.cpc.2006.03.005.

[80] M. Barhoumi, I. Said, N. Sfina, N. K. Al-Saleem, and T. Ghrib. A dft study of the electronic and optical properties of four 2d thin films. *Materials Chemistry and Physics*, 286:126158, 2022.
DOI: https://doi.org/10.1016/j.matchemphys.2022.126158.

[81] M. Jamal, S. Shahriyar Nishat, and A. Sharif. Effects of transition metal (fe, co and ni) doping on structural, electronic and optical properties of cuo: Dft + u study. *Chemical Physics*, 545:111160, 2021.
DOI: https://doi.org/10.1016/j.chemphys.2021.111160.

[82] E. Maskar, A. F. Lamrani, M. Belaiche, A. Es-Smairi, T. V. Vu, and D. P. Rai. A dft study of electronic, magnetic, optical and transport properties of rare earth element (gd, sm)-doped gan material. *Materials Science in Semiconductor Processing*, 139:106326, 2022.
DOI: https://doi.org/10.1016/j.mssp.2021.106326.

[83] A. Bafekry, C. Stampfl, and F. M. Peeters. The electronic, optical, and thermoelectric properties of monolayer pbte and the tunability of the electronic structure by external fields and defects. *physica status solidi (b)*, 257:2000182, 2020.
DOI: https://doi.org/10.1002/pssb.202000182.

[84] N. Amrane, M. Benkraouda, and Z. Mahdjoub. First principles calculations of optical properties of pbse, pbs and the alloy. *International Journal of Advanced Studies in Computers, Science and Engineering*, 2:23–30, 2013.

[85] C. M. I. Okoye. Electronic and optical properties of snte and gete. *Journal of Physics: Condensed Matter*, 14:8625, 2002.
DOI: https://doi.org/10.1088/0953-8984/14/36/318.

[86] H. Salehi, H. R. Zare, and P. Amiri. Investigation of optical and electronicproperties of cusbx2 (x=se, s, te) compounds in the surface state at(001) direction using density functional theory. *Iranian Journal of Surface Science and Engineering*, 13:67–75, 2017.
DOI: https://doi.org/20.1001.1.23222352.1400.10.0.11.4.